arXiv:1606.02093v2 [hep-ph] 26 Sep 2016

Measuring the trilinear neutral Higgs boson couplings in the minimal supersymmetric standard model at e^+e^- colliders in the light of the discovery of a Higgs boson

Charanjit K. Khosa and P. N. Pandita

Centre for High Energy Physics, Indian Institute of Science, Bangalore 560 012, India

(Dated: September 27, 2016)

Abstract

We consider the measurement of the trilinear couplings of the neutral Higgs bosons in the Minimal Supersymmetric Standard Model (MSSM) at a high energy e^+e^- linear collider in the light of the discovery of a Higgs boson at the CERN Large Hadron Collider (LHC). We identify the state observed at the LHC with the lightest Higgs boson (h^0) of the MSSM, and impose the constraints following from this identification, as well as other experimental constraints on the MSSM parameter space. In order to measure trilinear neutral Higgs couplings, we consider different processes where the heavier Higgs boson (H^0) of the MSSM is produced in electron-positron collisions, which subsequently decays into a pair of lighter Higgs boson. We identify the regions of the MSSM parameter space where it may be possible to measure the trilinear couplings of the Higgs boson at a future electron positron collider. A measurement of the trilinear Higgs couplings is a crucial step in the construction of the Higgs potential, and hence in establishing the phenomena of spontaneous symmetry breaking in gauge theories.

PACS numbers: 12.60.Jv, 14.80.Da, 14.80.Ly

Keywords: Trilinear Higgs Couplings, MSSM, LHC, Linear Collider

I. INTRODUCTION

The ATLAS [1] and CMS [2] experiments at the CERN Large Hadron Collider have independently observed a resonance at about 125-126 GeV. The ATLAS experiment after collecting data at an integrated luminosity of 4.8 fb^{-1} at $\sqrt{s} = 7$ TeV, and 5.8 fb^{-1} at $\sqrt{s} = 8$ TeV confirmed the evidence for the production of a neutral boson with a measured mass of $126.0 \pm 0.4(\text{stat}) \pm 0.4(\text{syst})$ GeV, with a significance of 5.9 σ. The CMS experiment after collecting 5.1 fb^{-1} at 7 TeV, and 5.3 fb^{-1} at 8 TeV reported an evidence of a neutral boson at $125.3 \pm 0.4(\text{stat}) \pm 0.5(\text{syst})$ GeV, with a significance of 5.8 σ. The CMS and ATLAS collaborations have now combined their analysis, which leads to the mass of the reported resonance as [3]

$$m_h \;=\; 125.09 \pm 0.21(\text{stat}) \pm 0.11(\text{syst})\ \text{GeV}. \tag{1}$$

The properties of the discovered state are consistent with the properties of the standard model (SM) Higgs boson. Nevertheless, this discovery opens up the possibility of searches for new physics beyond the standard model. Since the Higgs sector suffers from the problems of naturalness and hierarchy, a light Higgs boson is technically unnatural in standard model. Supersymmetry (SUSY) [4] is at present the leading candidate for physics beyond the SM in which a light Higgs boson, as discovered at the CERN LHC, is technically natural. The simplest implementation [5, 6] of the idea of supersymmetry at weak scale is the minimal supersymmetric standard model (MSSM). In MSSM the Higgs sector is more complex than the SM Higgs sector, and consists of two Higgs doublet superfields (H_1 and H_2). After gauge symmetry breaking the physical Higgs sector consists of two CP-even Higgs bosons ($h^0, H^0; m_{h^0} < m_{H^0}$), one CP-odd Higgs boson (A^0), and two charged states ($H^\pm$). Although gauge invariance and supersymmetry fix the quartic couplings of the Higgs bosons in the MSSM in terms of the $SU(2)_L$ and $U(1)_Y$ gauge couplings, g and g', respectively, there remain two independent parameters that describe the Higgs sector of the MSSM. These are conveniently chosen to be the mass of the CP-odd Higgs boson (m_{A^0}), and the ratio of the vacuum expectation values of the neutral components of the two Higgs fields, $\tan\beta \equiv < H_2^0 > / < H_1^0 >$. All the Higgs boson masses and the Higgs couplings in the MSSM can, then, be described, at the tree level, in terms of these two parameters. Discovery of more than one Higgs boson will, thus, be an indication of an extension of the SM, SUSY being the most favored candidate. It is, therefore, important to try to discover an extended

Higgs sector, if it exists, at the LHC. On the other hand it is also crucial to discover the supersymmetric partners of the SM particles, including the squarks, gluinos and sleptons, as well as the neutralinos and charginos.

In the absence of any signal for supersymmetric partners of the SM particles, it is appropriate to ask the question whether nonobservation of an extended Higgs sector would imply that the new physics is at a much higher energy scale. This question is related to the decay patterns [7–9] of the Higgs bosons of MSSM. This in turn is dependent on the Higgs couplings in the MSSM, and their deviation from the corresponding SM Higgs couplings. Apart from the couplings of Higgs bosons to the SM particles, which can be different from those of the corresponding SM Higgs couplings, the trilinear Higgs couplings can be very different in MSSM as compared to the SM trilinear Higgs coupling.

The measurement of the trilinear Higgs couplings [10–15] is an important step in the reconstruction of the Higgs potential, and thereby confirm the Higgs mechanism as the origin of the spontaneous breaking of the gauge symmetries in the SM (and in MSSM). As explained above, the tree level Higgs sector of the MSSM is described by only two parameters (m_{A^0} and $\tan\beta$). At the tree level the trilinear Higgs self couplings of the MSSM can also be described in terms of the same two parameters. In this paper we consider the question of measurement of the trilinear Higgs couplings in the MSSM at a high energy electron-positron collider in the light of the observation of the Higgs boson at the CERN LHC, which we identify with the lightest Higgs boson of the MSSM.

The plan of this paper is as follows. In Section II we recall the basic features of the Higgs sector of the minimal supersymmetric standard model and discuss the implications of the 125 GeV Higgs identification for the mass of the heavier Higgs boson (H^0) of the model, especially its dependence on the parameter space of the MSSM. In Section III we summarize the tree level as well as radiatively corrected trilinear Higgs couplings in the MSSM and discuss their dependence on the different parameters. In Section IV, we estimate the cross-section for different heavy Higgs production processes and discuss its branching ratios to light Higgs pair in the MSSM parameter space. In Section V we highlight the regions in the $(m_{A^0}, \tan\beta)$ plane where some of the MSSM Higgs trilinear couplings can be measured. In Section VI we summarize our results and conclusions.

II. THE HIGGS SECTOR OF THE MINIMAL SUPERSYMMETRIC STANDARD MODEL

To begin with, and to have a proper perspective, we recall that the potential for the physical Higgs boson in the SM can be written as

$$V_{SM}^{h} = \lambda \left(\phi^2 - \frac{v^2}{2}\right)^2 = \frac{m_h^2}{2}h^2 + \lambda_{hhh}^{SM}\frac{h^3}{3!} + \lambda_{hhhh}^{SM}\frac{h^4}{4!}, \tag{2}$$

where $< \phi >= v/\sqrt{2} \approx 174$ GeV is the vacuum expectation value of the neutral component of the Higgs doublet $\left(\phi = (1/\sqrt{2})(v+h)^T\right)$, and m_h is the mass of the physical Higgs boson. The trilinear and quartic Higgs couplings in the standard model can, then, be written as (in units of $(\sqrt{2}G_F)^{1/2}m_Z^2 = 33.77$ GeV and $(\sqrt{2}G_F)m_Z^4 = 1140.52$ GeV^2, respectively)

$$\lambda_{hhh}^{SM} = \frac{3m_h^2}{m_Z^2} = 5.6454, \tag{3}$$

$$\lambda_{hhhh}^{SM} = \frac{3m_h^2}{m_Z^4} = 0.00068 \text{ GeV}^{-2}. \tag{4}$$

The Higgs sector of the minimal supersymmetric model consists of two Higgs superfields, H_1 and H_2, with opposite hypercharge (Y = -1, Y = 1, respectively). The mass matrix for the CP even Higgs bosons can be written as [16–18]

$$\begin{aligned}\mathcal{M}^2 = & \begin{bmatrix} m_{A^0}^2 \sin^2\beta + m_Z^2\cos^2\beta & -(m_Z^2 + m_{A^0}^2)\sin\beta\cos\beta \\ -(m_Z^2 + m_{A^0}^2)\sin\beta\cos\beta & m_{A^0}^2\cos^2\beta + m_Z^2\sin^2\beta \end{bmatrix} \\ & + \frac{3g^2}{16\pi^2 m_W^2}\begin{bmatrix} \Delta_{11} & \Delta_{12} \\ \Delta_{12} & \Delta_{22} \end{bmatrix},\end{aligned} \tag{5}$$

where the second matrix embodies the radiative corrections. The radiative corrections Δ_{ij} depend, besides the top- and bottom-quark and squark masses, on the Higgs(ino) bilinear parameter μ in the superpotential, the soft supersymmetry breaking trilinear couplings (A_t, A_b), and soft supersymmetry breaking scalar masses (m_Q, m_U, m_D), as well as on $\tan\beta$. The radiatively corrected CP-even masses are obtained by diagonalizing the 2×2 mass matrix (5). After diagonalization the masses and the mixing angle α in the CP even

Higgs sector can be written as

$$
\begin{aligned}
m^2_{h^0/H^0} &= \frac{1}{2}(m^2_{A^0} + m^2_Z + \Delta M^2_{11} + \Delta M^2_{22} \mp \sqrt{m^4_{A^0} + m^4_Z - 2m^2_{A^0} m^2_Z \cos 4\beta + \delta}), \\
\tan\alpha &= \frac{2\Delta M^2_{12} - (m^2_{A^0} + m^2_Z)\sin 2\beta}{\Delta M^2_{11} - \Delta M^2_{22} + (m^2_Z - m^2_{A^0})\cos 2\beta + \sqrt{m^4_{A^0} + m^4_Z - 2m^2_{A^0} m^2_Z \cos 4\beta + \delta}}, \\
\delta &= 4\Delta M^4_{12} + (\Delta M^2_{11} - \Delta M^2_{22})^2 - 2(m^2_{A^0} - m^2_Z)(\Delta M^2_{11} - \Delta M^2_{22})\cos 2\beta \\
&\quad -4(m^2_{A^0} + m^2_Z)\Delta M^2_{12} \sin 2\beta, \\
&\quad \Delta M^2_{ij} = \frac{3g^2}{16\pi^2 m^2_W}\Delta_{ij}, \qquad i,j = 1,2. \qquad (6)
\end{aligned}
$$

In the numerical calculations of the Higgs boson mass, we shall take into account the one-loop and leading two-loop radiative corrections [16–21]. We shall identify the lightest CP-even Higgs boson of the MSSM with the state discovered at the CERN LHC [1–3] at $m_{h^0} \approx 125$ GeV. Requiring that the production cross section of the 125 GeV Higgs boson decaying to two photons agrees with the one observed at the CERN LHC divides the MSSM Higgs parameter space into two distinct regimes [22]: (i) The nondecoupling regime where $m_{A^0} \leq 130$ GeV. In this region the heavier Higgs H^0 is SM-like, and the light Higgs h^0 and CP-odd Higgs A^0 are almost degenerate [23], with mass close to m_Z, while the charged Higgs bosons $H^\pm$ are nearly degenerate with H^0. For a discussion of this possibility and its phenomenological implications at the LHC, see e.g. [24–26]. (ii) The decoupling regime where $m_{A^0} > 300$ GeV. In this limit the light CP-even Higgs boson h^0 is SM-like, and all other physical Higgs bosons are heavy, and almost degenerate [27] with A^0. These decoupling properties are a generic feature of models with extended Higgs sectors.

The nondecoupling scenario has also been explored recently in context of LHC 8 TeV data [28]. But as far as measurement of MSSM Higgs bosons trilinear coupling is concerned, the decoupling scenario is a more viable scenario. Therefore, in the following we shall consider only the MSSM with decoupling scenario while discussing the trilinear Higgs couplings. The nondecoupling scenario is discussed in some detail in [8].

In order to identify the state observed at the CERN LHC with the lightest Higgs boson of the MSSM, we shall adjust the supersymmetry breaking soft trilinear parameter A_t so as to get m_{h^0} in the range 122-128 GeV, corresponding to a 3 GeV theoretical uncertainty in the Higgs mass calculations. Having fixed m_{h^0}, we have performed a numerical scan of the MSSM parameter space using CalcHEP [29] which uses SuSpect [30] for MSSM spectrum calculations. SuSpect checks the stability of potential and calculates the spectrum only

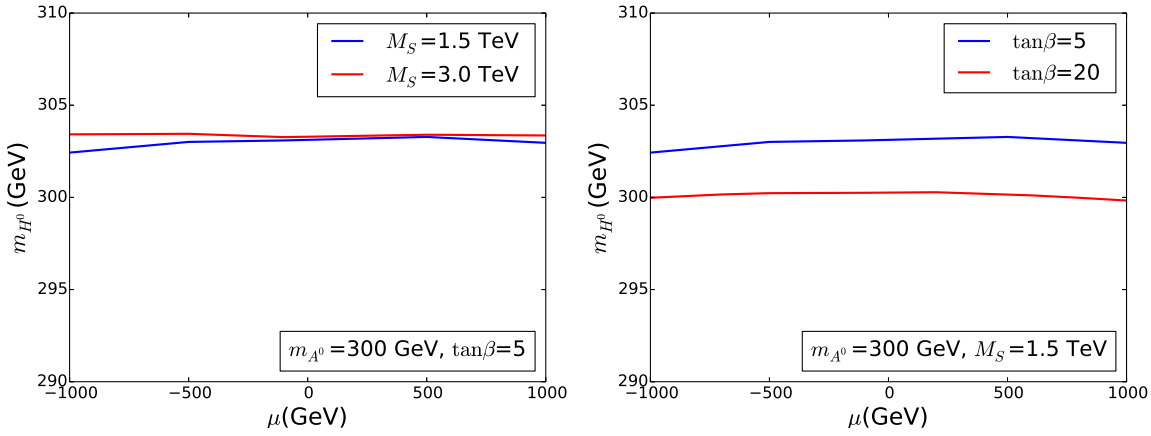

(a) (b)

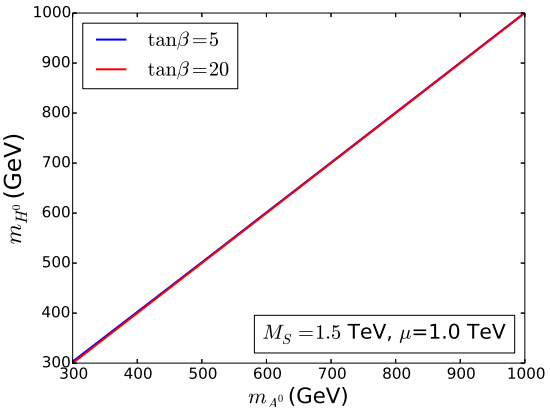

(c)

FIG. 1: The mass of heavier Higgs boson m_{H^0} as a function of (a) μ for fixed $\tan\beta$; (b) as a function of μ for fixed M_S; and (c) as a function of m_{A^0} for the values of the other parameters as shown in the inset. Soft trilinear parameter (A_t) is adjusted to get lightest Higgs boson (h^0) mass in 122-128 GeV range.

for stable points. For our analysis we use set of input parameters which are consistent with known experimental constraints, and also which have the possibility of leading to the supersymmetry spectra that may be observable in the upcoming experiments. We do this in order to have low energy supersymmetry as a viable option for solving the naturalness and hierarchy problem of the standard model. Using this procedure, we have calculated the dependence of the heavy CP-even Higgs boson mass m_{H^0} on μ for different values of $\tan\beta$, and the SUSY breaking scale M_S, which is defined to be $\sqrt{m_{\tilde{t_1}} m_{\tilde{t_2}}}$, where $m_{\tilde{t_1}}$ and $m_{\tilde{t_2}}$ are the masses of the two stop states. This dependence is shown in Fig.1. This Fig. shows that

μ in GeV	A_t in GeV	m_{h^0} in GeV
-1000	3845	123.25
-500	3845	123.61
500	3545	123.86
1000	3545	123.09

TABLE I: Values of μ, A_t and Higgs mass for M_S=1.5 TeV, m_{A^0}=300 GeV and $\tan\beta$=5.

m_{H^0} does not depend significantly on μ. For a given value of $\tan\beta$ it depends weakly on M_S. However, m_{H^0} has a significant dependence on m_{A^0} and $\tan\beta$, and can be described in terms of these two parameters to a good accuracy when we use the fact that m_{h^0} lies in the range 122-128 GeV. As an example, for one set of M_S, $\tan\beta$ and m_{A^0} we show the values of the parameter A_t with different values of μ in Table I. For the considered range of μ, A_t does not change much. For M_S=1.5 TeV, typical range of A_t is 2500-4000 GeV depending on $\tan\beta$.

III. TRILINEAR HIGGS BOSON COUPLINGS IN THE MINIMAL SUPERSYMMETRIC STANDARD MODEL

We now discuss the question of the measurement of trilinear couplings of the neutral Higgs bosons (h^0, H^0) of the minimal supersymmetric standard model. These couplings receive contributions at the tree level as well as from radiative corrections. We shall assume CP conservation throughout in this paper. Then the trilinear couplings can be written as[31]

$$\begin{aligned}
\lambda_{hhh} &= \lambda^0_{hhh} + \Delta\lambda_{hhh}, \\
\lambda_{Hhh} &= \lambda^0_{Hhh} + \Delta\lambda_{Hhh}, \\
\lambda_{hAA} &= \lambda^0_{hAA} + \Delta\lambda_{hAA}, \\
\lambda_{HAA} &= \lambda^0_{HAA} + \Delta\lambda_{HAA}, \\
\lambda_{HHH} &= \lambda^0_{HHH} + \Delta\lambda_{HHH}, \\
\lambda_{HHh} &= \lambda^0_{HHh} + \Delta\lambda_{HHh}, \qquad (7)
\end{aligned}$$

where λ^0's are the tree level values of the couplings, and $\Delta\lambda$'s are the radiative corrections. In this paper we shall consider the one-loop approximation for the radiative corrections to the trilinear Higgs couplings. The leading two loop SUSY-QCD corrections to the trilinear couplings are available in the literature [32] which reduces the scale dependence of one-loop corrections but the contribution is very small as compared to the one-loop corrections. The tree-level couplings in units of $(\sqrt{2}G_F)^{1/2}m_Z^2$ can be written as

$$\begin{aligned}
\lambda^0_{hhh} &= 3\cos 2\alpha \sin(\beta+\alpha), \\
\lambda^0_{Hhh} &= 2\sin 2\alpha \sin(\beta+\alpha) - \cos 2\alpha \cos(\beta+\alpha), \\
\lambda^0_{hAA} &= \cos 2\beta \sin(\beta+\alpha), \\
\lambda^0_{HAA} &= -\cos 2\beta \cos(\beta+\alpha), \\
\lambda^0_{HHH} &= 3\cos 2\alpha \cos(\beta+\alpha), \\
\lambda^0_{HHh} &= -2\sin 2\alpha \cos(\beta+\alpha) - \cos 2\alpha \sin(\beta+\alpha),
\end{aligned} \tag{8}$$

where α is the mixing angle in the CP-even Higgs sector, which can be obtained from the diagonalization of mass matrix (5), as shown in (6). The radiative corrections $\Delta\lambda$'s in (7) are summarized in the Appendix.

We note that the Higgs sector depends on five parameters in the MSSM, m_{A^0} and $\tan\beta$ from tree level mass matrix, and three parameters A_t, μ and M_S from radiative corrections. Of these M_S is fixed from nonobservation of colored particles to be greater than 1.5 TeV, and A_t is used to fix the value of lightest Higgs mass (m_{h^0}). For fixed value of $\tan\beta$ we are left with two parameters m_{A^0} and μ. In Fig. 2 we show the variation of radiatively corrected trilinear couplings with respect to m_{A^0} (for fixed value of μ), and with respect to μ (for fixed value of m_{A^0}), respectively. In Fig. 2 (c) we show the trilinear couplings as a functions of $\tan\beta$ (for fixed value of μ and m_{A^0}). Most of the variation in the trilinear Higgs couplings comes from the variation of the radiative corrections, a fact which is shown in Fig. 3, where we plot only the radiative corrections to different trilinear Higgs couplings.

From these Figures, we can see that the trilinear couplings are sensitive to m_{A^0} upto 500 GeV except the ones involving CP-odd Higgs boson. In Fig. 2 (c), we have shown the variation of trilinear Higgs couplings as a function of $\tan\beta$ for a value of $m_{A^0} = 300$ GeV, with other parameters kept fixed, and this plot shows that trilinear couplings are weakly dependent on $\tan\beta$. In this paper we shall consider only the trilinear couplings λ_{hhh} and λ_{Hhh} between the neutral Higgs bosons h^0 and H^0.

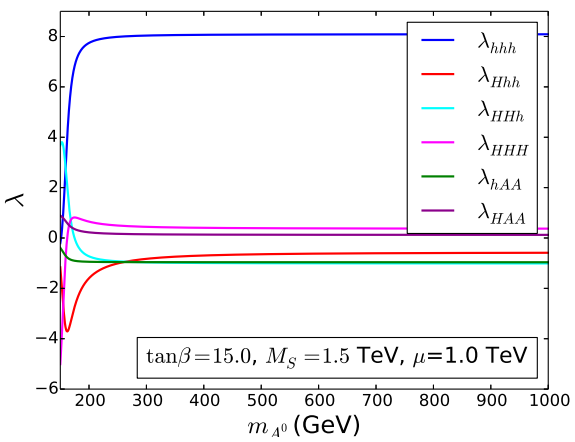

(a)

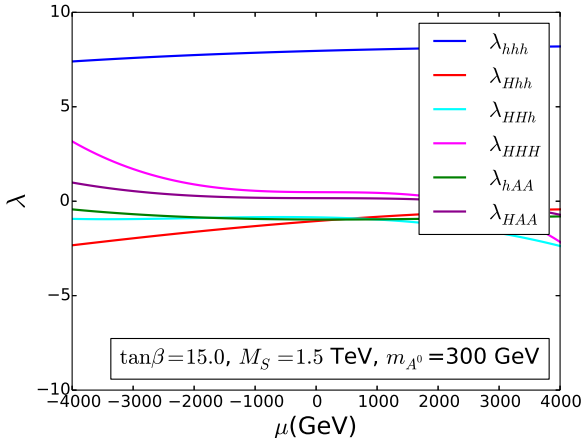

(b)

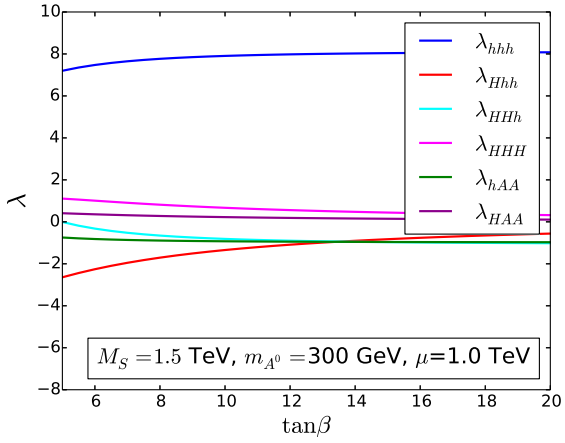

(c)

FIG. 2: Variation of radiatively corrected trilinear couplings in MSSM as functions of (a) m_{A^0}; (b) μ ; and (c) $\tan\beta$ for the values of the parameters as shown in the inset. In all the figures the soft trilinear parameter (A_t) is adjusted to obtain the value of the lightest Higgs boson mass in 122-128 GeV range. In this Fig. and in the following we have taken M_S =1.5 TeV.

IV. HIGGS PRODUCTION ANALYSIS

We now consider the different processes at an e^+e^- collider which can be used for the measurements of the trilinear Higgs couplings λ_{hhh} and λ_{Hhh} in the MSSM. These processes involve production of multiple Higgs bosons, to which we now turn.

Multiple light Higgs bosons (h^0) can be produced through heavy CP-even Higgs boson decays. For CP-even heavy Higgs boson production we consider Higgs-strahlung $e^+e^- \to ZH$,

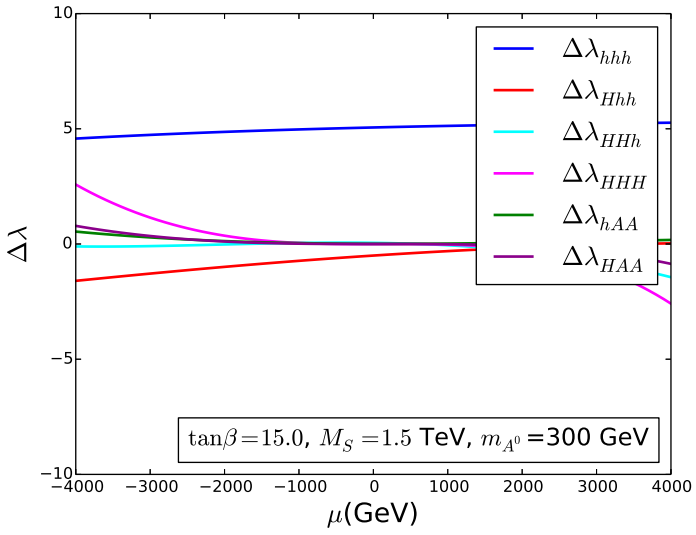

FIG. 3: Variation of the radiative corrections to the trilinear Higgs couplings ($\Delta\lambda$'s), in units of $(\sqrt{2}G_F)^{1/2}m_Z^2$, in MSSM as a function of μ for the fixed values of the other parameters as shown in the inset. The value of A_t is adjusted to get lightest Higgs boson mass in 122-128 GeV range.

associated production with CP-odd Higgs boson $e^+e^- \to AH$, and WW fusion mechanism $e^+e^- \to \nu_e\bar{\nu}_e H$. Feynman diagrams for these processes are shown in Figs. 4 and 5. Heavy Higgs boson H^0 subsequently decays to a pair of light Higgs bosons. The branching ratio of $H \to hh$ depends on trilinear Higgs coupling λ_{Hhh},

$$\Gamma(H \to hh) = \frac{G_F \lambda_{Hhh}^2}{16\sqrt{2}\pi} \frac{m_Z^4}{m_{H^0}} (1 - 4\frac{m_{h^0}^2}{m_{H^0}^2})^{1/2}. \tag{9}$$

Notice that this decay is kinematically forbidden in the non decoupling regime. The cross-sections for the Higgs-strahlung and associated production with CP-odd Higgs boson can be written as [11–13, 33, 34]

$$\sigma(e^+e^- \to ZH) = \frac{G_F^2 m_Z^4}{96\pi s}(v_e^2 + a_e^2)\cos^2(\beta-\alpha)\frac{\lambda_Z^{1/2}\left[\lambda_Z + 12m_Z^2/s\right]}{(1 - m_Z^2/s)^2}, \tag{10}$$

$$\sigma(e^+e^- \to AH) = \frac{G_F^2 m_Z^4}{96\pi s}(v_e^2 + a_e^2)\sin^2(\beta-\alpha)\frac{\lambda_A^{3/2}}{(1 - m_Z^2/s)^2}, \tag{11}$$

where λ_i is the phase-space function, which corresponds to $\lambda(m_i^2, m_{H^0}^2; s)$, and is given by

$$\lambda(m_a^2, m_b^2; m_c^2) = \left(1 - \frac{m_a^2}{m_c^2} - \frac{m_b^2}{m_c^2}\right)^2 - \frac{4m_a^2 m_b^2}{m_c^4}, \tag{12}$$

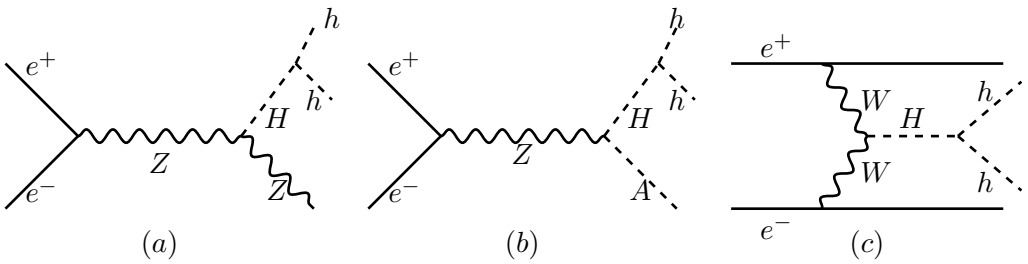

FIG. 4: Feynman diagrams for resonant production of hh, through $e^+e^- \to HZ$, HA, $\nu_e\bar{\nu}_e H$, where $H \to hh$ in the final state.

and $v_e = 4\sin^2\theta_W - 1$, $a_e = -1$ are the Z boson-electron couplings.

On the other hand resonant WW fusion cross-section for the light Higgs pair production can be written as [11–13]

$$\sigma(e^+e^- \to H\bar{\nu}_e\nu_e) = \frac{G_F^3 m_W^4}{64\sqrt{2}\pi^3}\left[\int_{\mu_H}^1 dx \int_x^1 \frac{dy}{\left[1+(y-x)/\mu_W\right]^2}\,\mathcal{F}(x,y)\right]\cos^2(\beta-\alpha), \quad (13)$$

where

$$\mathcal{F}(x,y) = 16[F(x,y)+G(x,y)], \quad (14)$$

$$F(x,y) = \left[\frac{2x}{y^3} - \frac{1+2x}{y^2} + \frac{2+x}{2y} - \frac{1}{2}\right]\left[\frac{z}{1+z} - \log(1+z)\right] + \frac{x}{y^3}\frac{z^2(1-y)}{(1+z)}, \quad (15)$$

$$G(x,y) = \left[-\frac{x}{y^2} + \frac{2+x}{2y} - \frac{1}{2}\right]\left[\frac{z}{1+z} - \log(1+z)\right], \quad (16)$$

with

$$\mu_H = \frac{m_{H^0}^2}{s}, \qquad z = \frac{y(x-\mu_H)}{\mu_W x}. \quad (17)$$

The multiple Higgs production through non resonant $WW \to hh$ proceeds via the diagrams shown in the Fig. 5. The non-resonant fusion $WW \to hh$ cross-section in the effective WW approximation can be written as

$$\sigma(e^+e^- \to \nu_e\bar{\nu}_e hh) = \int_\tau^1 \mathrm{d}x\,\frac{\mathrm{d}L}{\mathrm{d}x}\,\hat{\sigma}_{WW}(x), \quad (18)$$

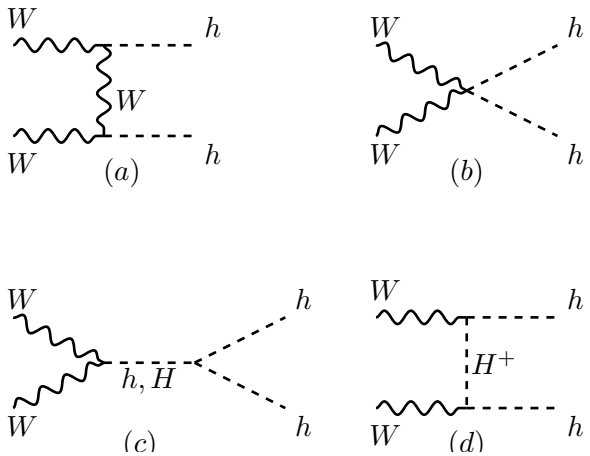

FIG. 5: Feynman diagrams for hh production through non-resonant WW fusion.

where

$$\tau = \frac{4m_{h^0}^2}{s}, \tag{19}$$

$$\frac{\mathrm{d}L(x)}{\mathrm{d}x} = \frac{G_{\mathrm{F}}^2 m_W^4}{2}\left(\frac{v^2+a^2}{4\pi^2}\right)^2 \frac{1}{x}\left\{(1+x)\log\frac{1}{x} - 2(1-x)\right\}, \tag{20}$$

and $\hat{\sigma}_{WW}(x)$ can be written as [11–13]

$$\begin{aligned}\hat{\sigma}_{WW}(x) = \frac{G_{\mathrm{F}}^2\hat{s}}{64\pi}\beta_h\Bigg\{&4\left[\frac{\hat{\mu}_Z\sin(\beta-\alpha)}{1-\hat{\mu}_h}\lambda_{hhh} + \frac{\hat{\mu}_Z\cos(\beta-\alpha)}{1-\hat{\mu}_H}\lambda_{Hhh} + 1\right]^2 g_0 \\ &+ \frac{2}{\beta_h}\left[\frac{\hat{\mu}_Z\sin(\beta-\alpha)}{1-\hat{\mu}_h}\lambda_{hhh} + \frac{\hat{\mu}_Z\cos(\beta-\alpha)}{1-\hat{\mu}_H}\lambda_{Hhh} + 1\right] \\ &\times\left[\sin^2(\beta-\alpha)\,g_1 + \cos^2(\beta-\alpha)\,g_2\right] \\ &+ \frac{1}{\beta_h^2}\{\sin^4(\beta-\alpha)\,g_3 + \cos^4(\beta-\alpha)\,g_4 + \sin^2[2(\beta-\alpha)]\,g_5\}\Bigg\},\end{aligned} \tag{21}$$

where

$$\hat{\mu}_i = \frac{m_i^2}{\hat{s}}\ (i = W, Z, h^0, H^0), \quad \beta_h = (1-4\hat{\mu}_h)^{1/2}, \quad \hat{s} = xs, \tag{22}$$

and the exact forms of g_i (i=0,..5) functions can be found in [11–13]. We note that there can be sizable deviations of the effective WW approximation from the exact result. However, we shall use this approximation as an estimate in this paper.

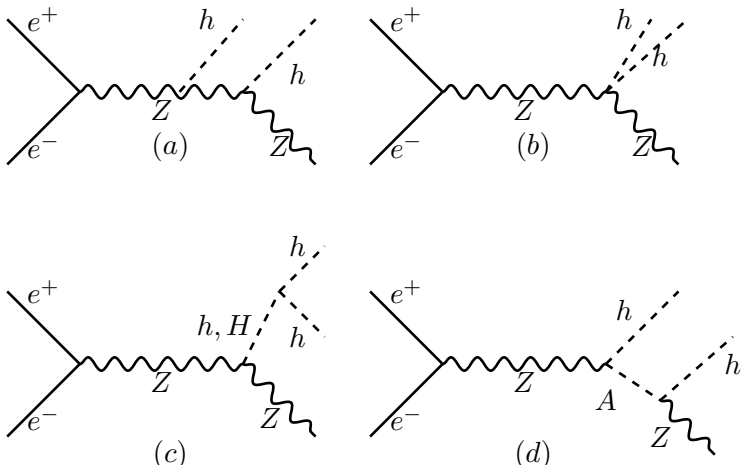

FIG. 6: Feynman diagrams for the non-resonant hh production in association with Z.

The off-shell Z boson decay

$$e^+e^- \to Z^* \to Zhh, \tag{23}$$

is another mechanism of hh production. Feynman diagrams for this process are shown in Fig. 6, and the cross-section is given by [11–13]

$$\frac{d\sigma(e^+e^- \to Zhh)}{dx_1 dx_2} = \frac{G_F^3 m_Z^6}{384\sqrt{2}\pi^3 s}(v_e^2 + a_e^2)\frac{\mathcal{A}}{(1-\mu_Z)^2}, \tag{24}$$

where $x_{1,2} = 2E_{1,2}/\sqrt{s}$ are the scaled energies of the Higgs particles, $x_3 = 2 - x_1 - x_2$ for the scaled energy of the Z boson, and $y_k = 1 - x_k$. Also, $\mu_i = m_i^2/s$ denotes the scaled squared masses of various particles:

$$\mu_h = m_{h^0}^2/s, \qquad \mu_H = m_{H^0}^2/s, \qquad \mu_W = m_W^2/s, \tag{25}$$

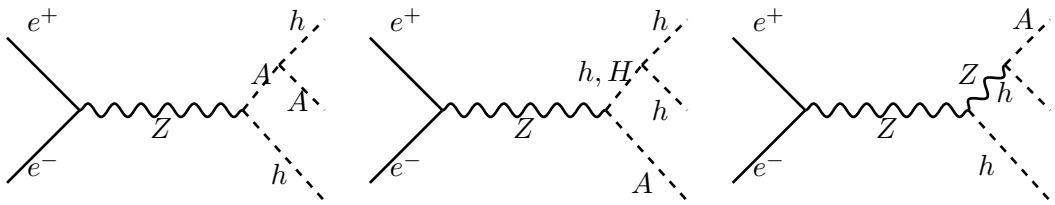

FIG. 7: Feynman diagrams for the non-resonant hh production in association with A.

and

$$\mathcal{A} = \mu_Z \left\{ \tfrac{1}{2}|a|^2 f_a + |b(y_1)|^2 f_b + 2\,\mathrm{Re}[ab^*(y_1)]\, g_{ab} + \mathrm{Re}[b(y_1)b^*(y_2)]\, g_{bb} \right\} + \{x_1 \leftrightarrow x_2\}. \quad (26)$$

Here

$$a = \frac{1}{2}\left[\frac{\sin(\beta-\alpha)\lambda_{hhh}}{y_3+\mu_Z-\tilde{\mu}_h} + \frac{\cos(\beta-\alpha)\lambda_{Hhh}}{y_3+\mu_Z-\tilde{\mu}_H}\right] + \left[\frac{\sin^2(\beta-\alpha)}{y_1+\mu_h-\tilde{\mu}_Z} + \frac{\sin^2(\beta-\alpha)}{y_2+\mu_h-\tilde{\mu}_Z}\right] + \frac{1}{2\mu_Z}, \quad (27)$$

$$b(y) = \frac{1}{2\mu_Z}\left(\frac{\sin^2(\beta-\alpha)}{y+\mu_h-\tilde{\mu}_Z} + \frac{\cos^2(\beta-\alpha)}{y+\mu_h-\tilde{\mu}_A}\right). \quad (28)$$

and $\tilde{\mu}_Z = (m_Z^2 + i m_Z \Gamma_Z)/s$, which takes care of the widths. The Higgs self-couplings λ_{Hhh} and λ_{hhh} occur only in the function a, Eq. (27). The coefficients f and g do not involve any Higgs couplings and can be written as

$$\begin{aligned}
f_a &= x_3^2 + 8\mu_Z, \\
f_b &= (x_1^2 - 4\mu_h)[(y_1-\mu_Z)^2 - 4\mu_Z\mu_h], \\
g_{ab} &= \mu_Z[2(\mu_Z - 4\mu_h) + x_1^2 + x_2(x_2+x_3)] - y_1(2y_2 - x_1x_3), \\
g_{bb} &= \mu_Z^2(4\mu_h + 6 - x_1x_2) + 2\mu_Z(\mu_Z^2 + y_3 - 4\mu_h) \\
&\quad + (y_3 - x_1x_2 - x_3\mu_Z - 4\mu_h\mu_Z)(2y_3 - x_1x_2 - 4\mu_h + 4\mu_Z).
\end{aligned} \quad (29)$$

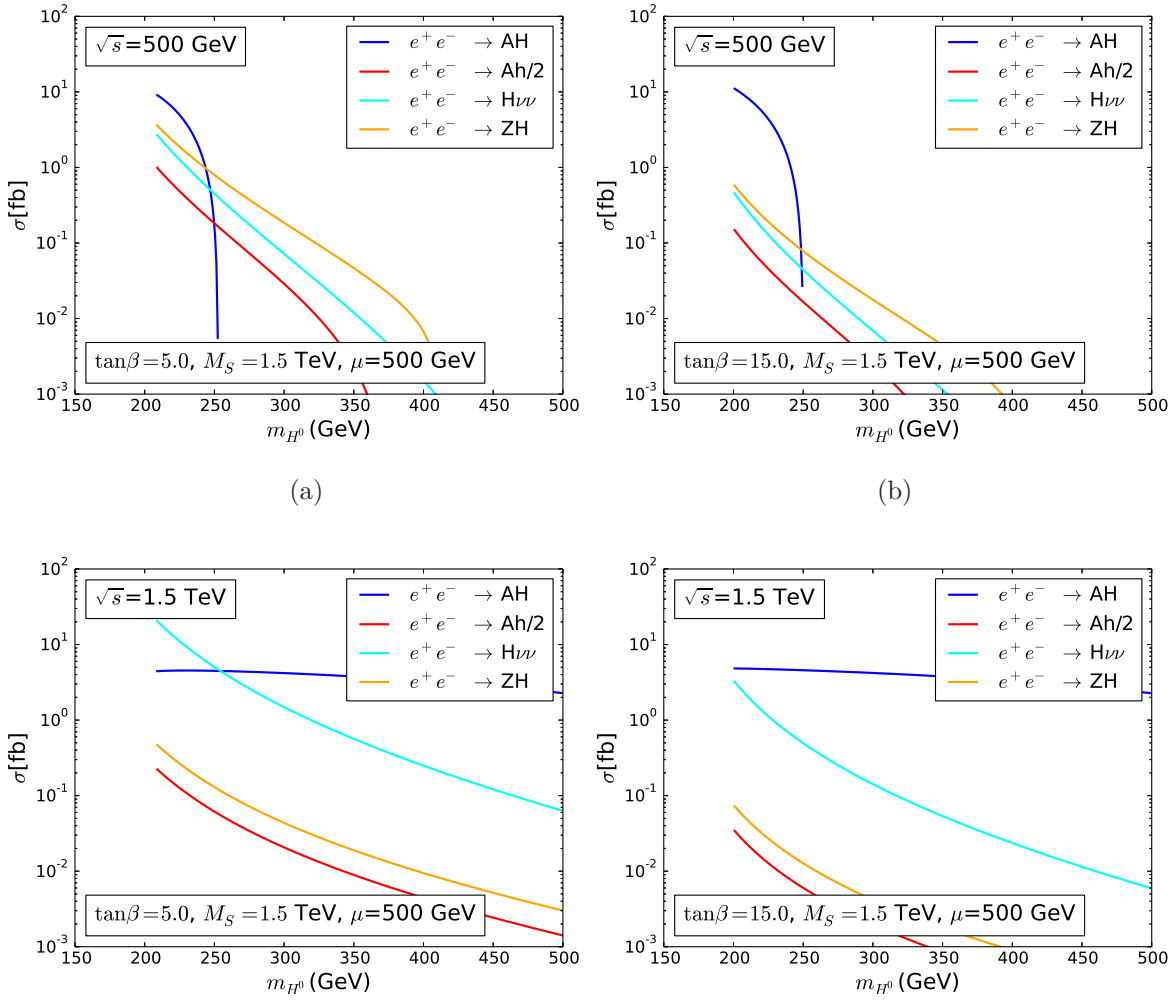

FIG. 8: Cross-section for $e^+e^- \to AH, ZH, Ah/2, H\nu\nu$ as the functions of m_{H^0} for $\sqrt{s} = 500$ GeV and $\sqrt{s} = 1.5$ TeV for values of other parameters as shown in the inset. Soft trilinear coupling A_t is adjusted to get light Higgs boson mass in 122-128 GeV range.

We note that the Feynman diagram Fig. 6(c) involves the trilinear Higgs couplings λ_{Hhh} and λ_{hhh}, whereas the other diagrams in Fig. 6 do not involve any trilinear Higgs couplings. The background to the multiple Higgs production process comes from pseudoscalar A production with h, where A subsequently decays to hZ (see Fig. 6(d) for the corresponding Feynman diagram)

$$e^+e^- \to Ah, \qquad A \to hZ. \tag{30}$$

The production cross-section for $e^+e^- \to Ah$ can be written as

μ (in GeV)	M_1 (in GeV)	M_2 (in GeV)	M_{χ^0} (in GeV)	$M_{\chi^\pm}$ (in GeV)
-230.0	120.0	240.0	$108.0, 181.7, 235.6, 305.9$	$173.5, 304.1$
-500.0	150.0	300.0	$146.9, 283.4, 503.2, 522.9$	$282.9, 521.6$

TABLE II: The neutralino and chargino mass spectrum for the benchmark values of the μ parameter and soft supersymmetric breaking gaugino masses M_1 and M_2.

$$\sigma(e^+e^- \to Ah) = \frac{G_F^2 m_Z^4}{96\pi s}(v_e^2 + a_e^2)\cos^2(\beta-\alpha)\frac{\lambda^{3/2}(m_{h^0}^2, m_{A^0}^2; s)}{(1-m_Z^2/s)^2}, \tag{31}$$

and decay width for $A \to hZ$ is given by

$$\Gamma(A \to hZ) = \frac{G_F}{8\pi\sqrt{2}}\cos^2(\beta-\alpha)\frac{m_Z^4}{m_{A^0}}\lambda^{1/2}(m_Z^2, m_{h^0}^2; m_{A^0}^2)\lambda(m_{A^0}^2, m_{h^0}^2; m_Z^2). \tag{32}$$

We note that the Feynman diagrams shown in Fig. 7 will lead to hhh final state through $A \to hZ$ decay, whereas we are interested in final states having hh final state.

In Fig. 8 we show the cross-section for $e^+e^- \to HZ$, HA, $H\nu\bar{\nu}$, (Fig.4), Ah (Fig. 6(d)) as a function of m_{H^0} for different values of $\sqrt{s}$ and $\tan\beta$. The heavy Higgs production with CP-odd Higgs is the dominant production channel for $m_{H^0} \leq 250$ GeV. We can see that $(\sigma(e^+e^- \to Ah))/2$ is of order of $\sigma(e^+e^- \to ZH)$ and $\sigma(e^+e^- \to H\nu\bar{\nu})$.

In Figs. 9 and 10, we show the branching fractions of heavy Higgs and pseudoscalar to different channels respectively for $\tan\beta = 5$, 10. In this paper we have also considered supersymmetric particles in the final states, consistent with current experimental constraints. All the SUSY particles have masses $\approx M_S$ except neutralinos and charginos. The neutralinos and charginos mass spectrum depends on the supersymmetry breaking gaugino mass parameters M_1 and M_2 as well as μ and $\tan\beta$. We recall that the chargino mass lower bounds from the LEP experiment imply [35]

$$|\mu|, M_2 \geq 100 \text{ GeV}. \tag{33}$$

We shall confine ourselves to the scenario where supersymmetry breaking gaugino masses M_i ($i = 1, 2, 3$) are equal at the grand unified scale. In this case the renormalization group evolution of M_i implies $M_1 \approx 0.5\ M_2$ at the weak scale. We shall consider the parameter space consistent with these constraints.

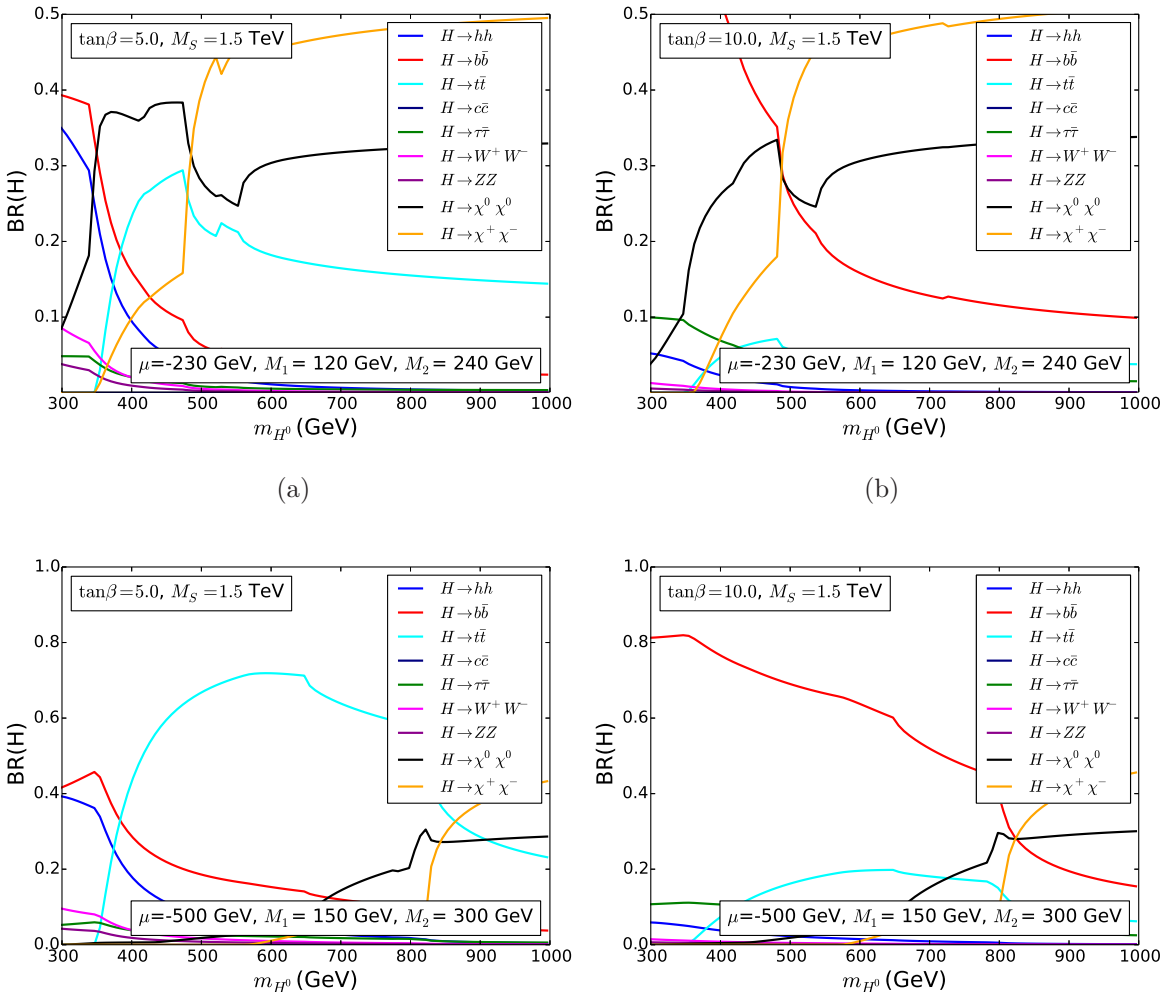

FIG. 9: The branching fractions for different decay channels of heavy Higgs (H) boson as a function of m_{H^0}, for the fixed values of parameters shown in the inset.

We have plotted the H and A branching fractions for two benchmark values of μ, M_1 and M_2. The neutralino and chargino mass spectrum for the benchmark points is given in Table II. The second benchmark point has comparatively heavy spectrum. We observe that for $m_{A^0} \approx m_{H^0} \geq 500$ GeV, neutralino and chargino are the dominant decay modes of both H and A, for a light neutralino and chargino spectrum. If these are heavy then $t\bar{t}$ is the dominant decay channel for low values of $\tan\beta$. In case of H decay, below $t\bar{t}$ threshold both $b\bar{b}$ and hh have appreciable branching fractions. For large $\tan\beta$ and heavy neutralino and chargino spectrum, $b\bar{b}$ is the dominant decay mode of the heavy Higgs boson as shown in Fig. 9 (d). Our aim is to study BR($H \to hh$) and BR($A \to hZ$), since the former involves the

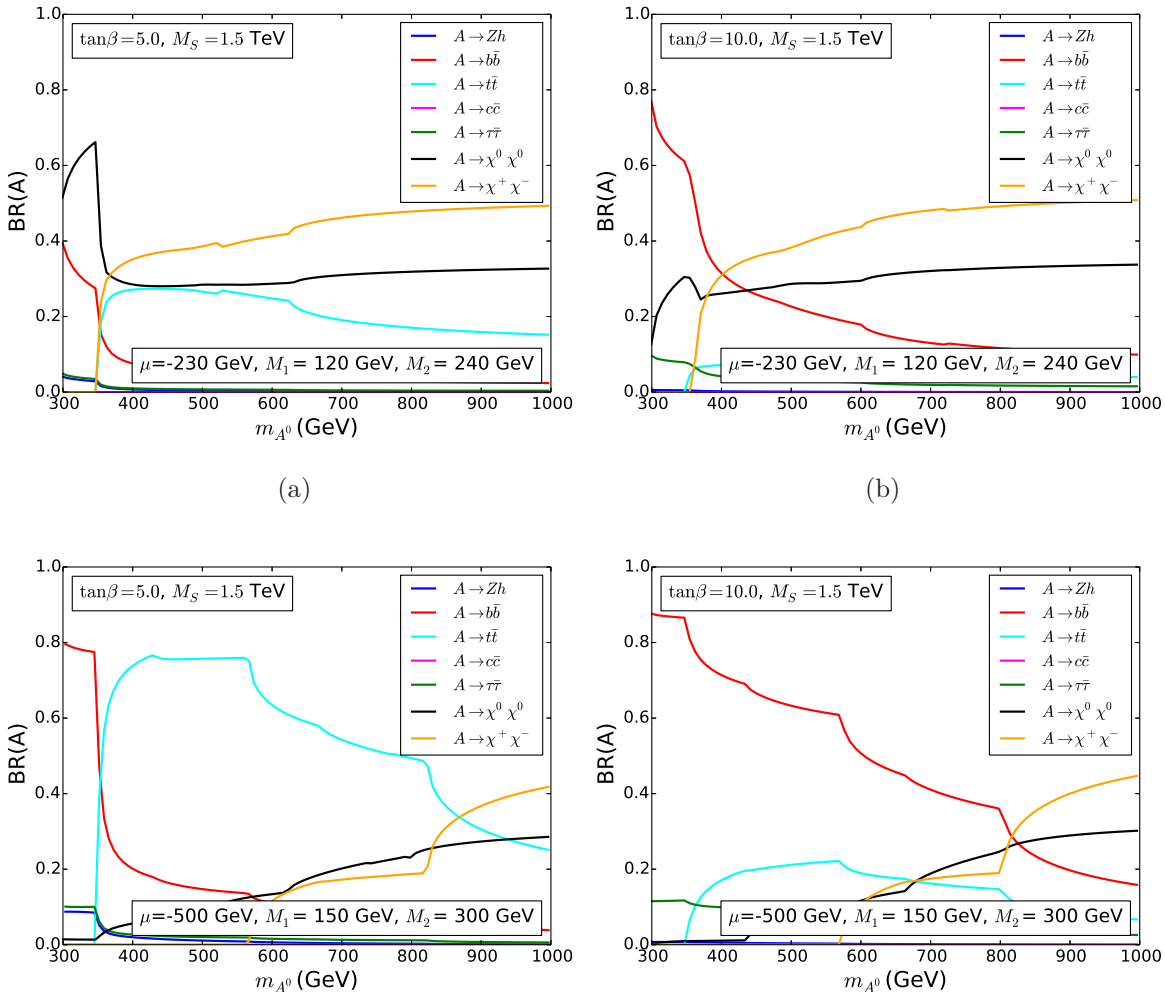

FIG. 10: Branching fractions for different decay channels of A as the functions of m_{A^0} for the fixed values of parameters shown in the inset.

Higgs trilinear coupling and latter is background for multiple Higgs production processes. We can see from Fig. 10 that $A \to hZ$ branching fraction is negligible for values of $\tan\beta =$ 5 and 10. Below $\chi^+\chi^-$ threshold, $A \to b\bar{b}$ is the dominant decay channel for large value of $\tan\beta$.

The contours of constant values of BR($H \to hh$) are shown in Fig. 11 for the benchmark points. The BR($H \to hh$) decreases with increasing $\tan\beta$. Since the neutralino and chargino spectrum is heavy for the second benchmark point, BR($H \to \chi^0\chi^0, \chi^+\chi^-$) is suppressed as compared to first benchmark point and consequently BR($H \to hh$) is enhanced. In all the plots we have varied the relevant parameters in a manner so that the lightest Higgs mass is

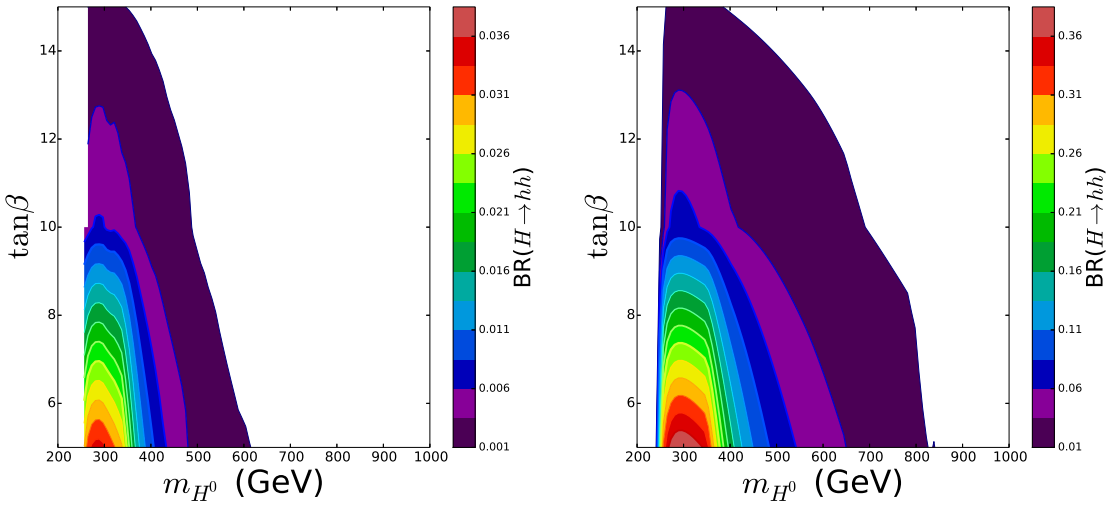

(a) (b)

FIG. 11: The contours of constant branching ratio for H decay to hh for (a) μ = -230 GeV, M_1 = 120 GeV and M_2 = 240 GeV, and (b) μ = -500 GeV, M_1 = 150 GeV and M_2 = 300 GeV. Other parameters are varied to get the lightest Higgs mass in 122-128 GeV range.

in the range 122-128 GeV. The main parameter adjusted in this context is A_t. As already mentioned we have allowed a 3 GeV theoretical uncertainty in the Higgs mass calculations. If one wants to restrict to the range of 124-126 GeV for the mass of the Higgs boson, then we will have a corresponding slightly narrow band of A_t values. In other words that will also reduce the range of values of the parameter A_t. But that minor variation in the A_t values will not change our analysis significantly since A_t parameter enters through one loop radiative corrections in the trilinear coupling calculations. Processes shown in Fig. 4 involve only trilinear coupling λ_{Hhh}, but Fig. 5 (c) and 6 (c) involve both λ_{hhh} and λ_{Hhh}. Therefore one has to study non-resonant multiple Higgs production cross-section to measure λ_{hhh} coupling.

V. MEASUREMENT OF TRILINEAR HIGGS COUPLINGS

In this Section we will compute the regions of (m_{A^0},tan β) plane where trilinear couplings λ_{Hhh} and λ_{hhh} can be measured. We calculate the heavy Higgs production cross-section using Eqs. 10, 11 and 13. The contours of $\sigma(H) \times BR(H \to hh)$ for $\sqrt{s}$ = 500 GeV and $\sqrt{s}$ = 1.5 TeV, respectively are shown in Fig. 12. In upper left and right panel, the

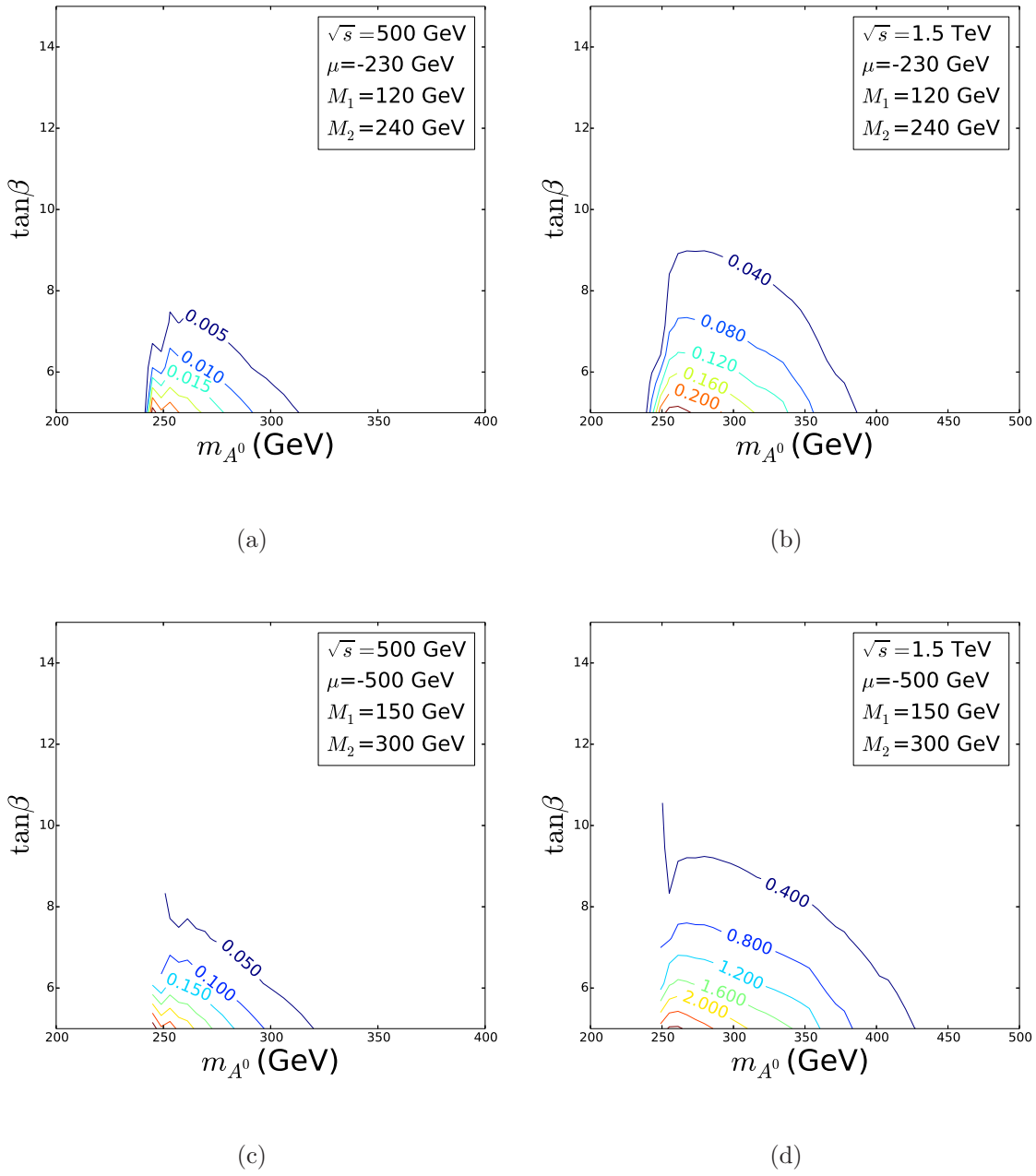

FIG. 12: The contours of constant $\sigma(H) \times BR(H \to hh)$ (in fb) for the values of the parameters shown in the inset.

outermost contours correspond to $\sigma(H) \times BR(H \to hh) \approx 0.005$ fb and .04 fb, respectively. The $\sigma(H) \times BR(H \to hh)$ decreases as we move diagonally upward in the (m_{A^0},tan β) plane because $BR(H \to hh)$ decreases in this direction. As shown in Fig. 8, the heavy Higgs production cross-section increases for $\sqrt{s} = 1.5$ TeV, therefore one can measure λ_{Hhh} coupling with a lower luminosity.

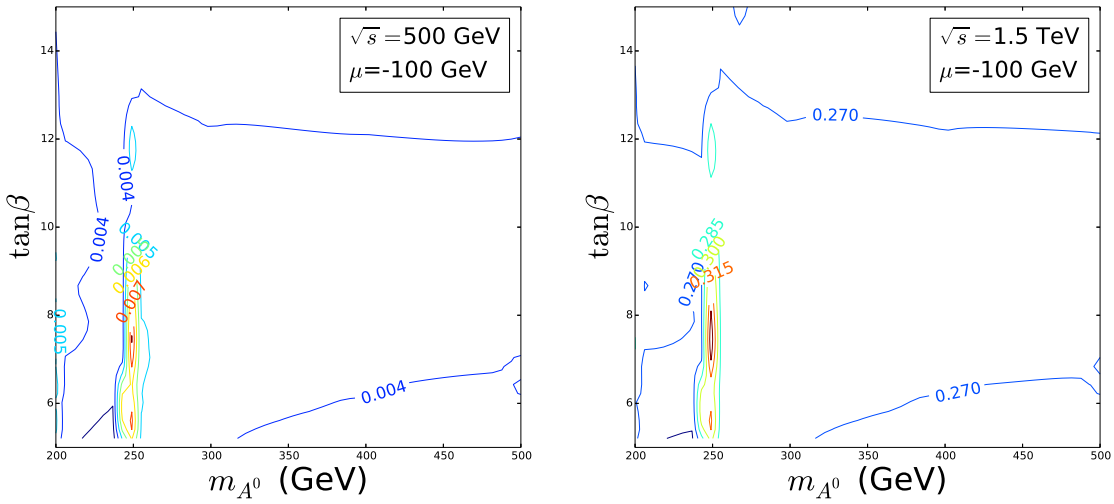

(a) (b)

FIG. 13: The contours of non-resonant $\sigma(ee \to hh\nu\bar{\nu})$ (in fb) via non-resonant WW fusion.

The BR($H \to hh$) is directly proportional to λ_{Hhh} and this branching ratio decreases with increasing $\tan\beta$ for fixed value of m_{A^0}. As discussed earlier, heavy Higgs production cross-section decreases with m_{A^0}. The H branching ratio to hh pair is kinematically forbidden for $m_{A^0} \approx m_{H^0} \leq 250$ GeV. Therefore, the lower left corner of (m_{A^0},$\tan\beta$) plane is the suitable region to measure λ_{Hhh} coupling. We can see from the Fig. 12 that $\sigma(H) \times BR(H \to hh)$ is sensitive to the μ parameter. In other words, precise knowledge of neutralino and chargino spectrum is crucial in order to determine the λ_{Hhh} coupling. For $\sqrt{s} = 1.5$ TeV and heavy neutralino and chargino spectrum with $\tan\beta \approx 10$, $\sigma(H) \times BR(H \to hh) \approx 0.4$ fb. This cross-section is 0.05 fb for $\sqrt{s}$=500 GeV so with a luminosity of 500 fb $^{-1}$, 25 events could be seen. This indicates only order of magnitude that can be reached but the actual number of events seen will be lowered by the efficiencies. The simulations of signal and background will depend on the detector sensitivity which is not the focus of this paper.

The $hh\nu_e\bar{\nu}_e$ final state produced through non-resonant WW fusion involves both λ_{hhh} and λ_{Hhh} coupling. Having an estimate of the coupling λ_{Hhh} from resonant WW production process, we can use non-resonant WW fusion process to measure the trilinear λ_{hhh} coupling. In Fig. 13 we show the constant contours of the cross-section for the non-resonant WW fusion process $\sigma(hh\nu_e\bar{\nu}_e)$ in the $(m_{A^0}, \tan\beta)$ plane. We can see that the cross-section $\sigma(hh\nu_e\bar{\nu}_e)$ is almost independent of the values of m_{A^0} and $\tan\beta$. The chances of the measurement of

λ_{hhh} are same in most of the $(m_{A^0}, \tan\beta)$ parameter space. There is a small increase in the cross-section at the boundary $m^2_{H^0} \approx 4\ m^2_{h^0}$ where Fig. 5(c) starts contributing through resonant process. Even with the 1000 fb $^{-1}$ of luminosity at $\sqrt{s} = 500$ GeV one could see only few events.

In Fig. 8 we have plotted the cross-section for the background process $e^+e^- \to Ah$ and BR $(A \to hZ)$ in Fig. 10. Since BR $(A \to hZ)$ is negligible this process will be suppressed for the considered parameter space. Also this kind of background events can be easily distinguished from the signal events by just looking at the hh pair invariant mass distribution which will resonate in case of signal process.

VI. CONCLUSIONS

We have carried out a detailed analysis of the measurement of trilinear couplings of the neutral CP-even Higgs boson, λ_{Hhh} and λ_{hhh}, at an electron-positron collider. For this purpose we have identified the state observed at CERN Large Hadron Collider at ≈ 125 GeV with the lightest Higgs boson of the MSSM. This identification has been used to study the dependence of the mass of the heavier CP-even Higgs boson of the MSSM (H^0) on the parameter space of the MSSM, so as to get a handle on the mass of H^0. Furthermore, we have also used the lower bound on the chargino mass from the LEP experiments to constrain the parameter space of the MSSM. All these constraints have been used in our study of the trilinear couplings.

Our main purpose is to investigate various processes involving multiple Higgs bosons in the final state in e^+-e^- collisions, consistent with the constraints summarized above. The production of the heavier Higgs bosons in e^+e^- collisions can lead to multiple lighter Higgs bosons (h^0) in the final state, which can be used in the measurement of the trilinear couplings of the CP-even Higgs bosons.

We indicate the regions of the $(m_{A^0}, \tan\beta)$ plane where trilinear coupling λ_{Hhh} and λ_{hhh} can be measured at the linear collider. The resonant heavy Higgs production processes are used to extract λ_{Hhh} coupling. For $\sqrt{s}$= 1.5 TeV, $\tan\beta \approx 8$, the $\sigma(H) \times BR(H \to hh)$ ≈ 1 fb, and regions of $\tan\beta$ upto 10 and m_{A^0} upto 450 can be explored for λ_{Hhh} coupling measurement. However high luminosity is required to probe larger $\tan\beta$ values. For the measurement of the λ_{hhh} coupling, we use light Higgs pair production through non-resonant

WW fusion, and this cross-section is not very sensitive to m_{A^0} and $\tan\beta$. Besides values of m_{A^0} and $\tan\beta$, the information of neutralino and chargino masses is crucial for determining the trilinear couplings.

VII. ACKNOWLEDGMENTS

The work of P. N. Pandita is supported by the Department of Atomic Energy, India through its Raja Ramanna Fellowship. He would like to thank the Inter University Centre for Astronomy and Astrophysics, Pune for hospitality where part of this work was done. C. K. Khosa would like to thank Jayita Lahiri for many fruitful discussions.

VIII. APPENDIX

In this Appendix we summarize the one-loop radiative corrections to the trilinear Higgs couplings in the MSSM [11–13, 31]. The radiative corrections, in units of $(\sqrt{2}G_F)^{1/2}m_Z^2$ can

be written as

$$\begin{aligned}
\Delta\lambda_{Hhh} &= \left(\frac{3g^2\cos^2\theta_W}{16\pi^2}\frac{m_t^4}{m_W^4}\frac{\sin\alpha\cos^2\alpha}{\sin^3\beta}\right) \\
&\times \left[3\log\frac{m_{\tilde{t}_1}^2 m_{\tilde{t}_2}^2}{m_t^4} + (m_{\tilde{t}_1}^2 - m_{\tilde{t}_2}^2)C_t(E_t+2F_t)\log\frac{m_{\tilde{t}_1}^2}{m_{\tilde{t}_2}^2}\right. \\
&\quad +2\left(\frac{m_t^2}{m_{\tilde{t}_1}^2}\left[1+(m_{\tilde{t}_1}^2 - m_{\tilde{t}_2}^2)C_tE_t\right]\left[1+(m_{\tilde{t}_1}^2 - m_{\tilde{t}_2}^2)C_tF_t\right]^2\right. \\
&\quad \left.\left. + \frac{m_t^2}{m_{\tilde{t}_2}^2}\left[1-(m_{\tilde{t}_1}^2 - m_{\tilde{t}_2}^2)C_tE_t\right]\left[1-(m_{\tilde{t}_1}^2 - m_{\tilde{t}_2}^2)C_tF_t\right]^2 - 2\right)\right], \qquad (34) \\
\Delta\lambda_{hhh} &= \left(\frac{3g^2\cos^2\theta_W}{16\pi^2}\frac{m_t^4}{m_W^4}\frac{\cos^3\alpha}{\sin^3\beta}\right) \\
&\times \left[3\log\frac{m_{\tilde{t}_1}^2 m_{\tilde{t}_2}^2}{m_t^4} + 3(m_{\tilde{t}_1}^2 - m_{\tilde{t}_2}^2)C_tF_t\log\frac{m_{\tilde{t}_1}^2}{m_{\tilde{t}_2}^2}\right. \\
&\quad \left. + 2\left(\frac{m_t^2}{m_{\tilde{t}_1}^2}\left[1+(m_{\tilde{t}_1}^2 - m_{\tilde{t}_2}^2)C_tF_t\right]^3 + \frac{m_t^2}{m_{\tilde{t}_2}^2}\left[1-(m_{\tilde{t}_1}^2 - m_{\tilde{t}_2}^2)C_tF_t\right]^3 - 2\right)\right], \qquad (35) \\
& \qquad (36) \\
\Delta\lambda_{hAA} &= \left(\frac{3g^2\cos^2\theta_W}{16\pi^2}\frac{m_t^4}{m_W^4}\frac{\cos\alpha\cos^2\beta}{\sin^3\beta}\right) \\
&\times \left[\log\frac{m_{\tilde{t}_1}^2 m_{\tilde{t}_2}^2}{m_t^4} + (m_{\tilde{t}_1}^2 - m_{\tilde{t}_2}^2)(D_t^2+C_tF_t)\log\frac{m_{\tilde{t}_1}^2}{m_{\tilde{t}_2}^2}\right. \\
&\quad \left. +(m_{\tilde{t}_1}^2 - m_{\tilde{t}_2}^2)^2 C_tD_t^2F_t\, g(m_{\tilde{t}_1}^2, m_{\tilde{t}_2}^2)\right], \qquad (37) \\
\Delta\lambda_{HAA} &= \left(\frac{3g^2\cos^2\theta_W}{16\pi^2}\frac{m_t^4}{m_W^4}\frac{\sin\alpha\cos^2\beta}{\sin^3\beta}\right) \\
&\times \left[\log\frac{m_{\tilde{t}_1}^2 m_{\tilde{t}_2}^2}{m_t^4} + (m_{\tilde{t}_1}^2 - m_{\tilde{t}_2}^2)(D_t^2+C_tE_t)\log\frac{m_{\tilde{t}_1}^2}{m_{\tilde{t}_2}^2}\right. \\
&\quad \left. +(m_{\tilde{t}_1}^2 - m_{\tilde{t}_2}^2)^2 C_tD_t^2E_t g(m_{\tilde{t}_1}^2, m_{\tilde{t}_2}^2)\right], \qquad (38)
\end{aligned}$$

$$
\begin{aligned}
\Delta\lambda_{HHH} &= \left(\frac{3g^2\cos^2\theta_W}{16\pi^2}\frac{m_t^4}{m_W^4}\frac{\sin^3\alpha}{\sin^3\beta}\right) \\
&\times \left[3\log\frac{m_{\tilde{t}_1}^2 m_{\tilde{t}_2}^2}{m_t^4} + 3(m_{\tilde{t}_1}^2 - m_{\tilde{t}_2}^2)C_tE_t\log\frac{m_{\tilde{t}_1}^2}{m_{\tilde{t}_2}^2}\right. \\
&\quad +2\left(\frac{m_t^2}{m_{\tilde{t}_1}^2}\left[1+(m_{\tilde{t}_1}^2 - m_{\tilde{t}_2}^2)C_tE_t\right]^3\right. \\
&\quad \left.\left. + \frac{m_t^2}{m_{\tilde{t}_2}^2}\left[1-(m_{\tilde{t}_1}^2 - m_{\tilde{t}_2}^2)C_tE_t\right]^3 - 2\right)\right], \qquad (39) \\
\Delta\lambda_{HHh} &= \left(\frac{3g^2\cos^2\theta_W}{16\pi^2}\frac{m_t^4}{m_W^4}\frac{\sin^2\alpha\cos\alpha}{\sin^3\beta}\right) \\
&\times \left[3\log\frac{m_{\tilde{t}_1}^2 m_{\tilde{t}_2}^2}{m_t^4} + (m_{\tilde{t}_1}^2 - m_{\tilde{t}_2}^2)C_t(2E_t+F_t)\log\frac{m_{\tilde{t}_1}^2}{m_{\tilde{t}_2}^2}\right. \\
&\quad +2\left(\frac{m_t^2}{m_{\tilde{t}_1}^2}\left[1+(m_{\tilde{t}_1}^2 - m_{\tilde{t}_2}^2)C_tE_t\right]^2\left[1+(m_{\tilde{t}_1}^2 - m_{\tilde{t}_2}^2)C_tF_t\right]\right. \\
&\quad \left.\left. + \frac{m_t^2}{m_{\tilde{t}_2}^2}\left[1-(m_{\tilde{t}_1}^2 - m_{\tilde{t}_2}^2)C_tE_t\right]^2\left[1-(m_{\tilde{t}_1}^2 - m_{\tilde{t}_2}^2)C_tF_t\right] - 2\right)\right], \qquad (40)
\end{aligned}
$$

where

$$
\begin{aligned}
C_t &= (A+\mu\cot\beta)/(m_{\tilde{t}_1}^2 - m_{\tilde{t}_2}^2), \\
D_t &= (A-\mu\tan\beta)/(m_{\tilde{t}_1}^2 - m_{\tilde{t}_2}^2), \\
E_t &= (A+\mu\cot\alpha)/(m_{\tilde{t}_1}^2 - m_{\tilde{t}_2}^2), \\
F_t &= (A-\mu\tan\alpha)/(m_{\tilde{t}_1}^2 - m_{\tilde{t}_2}^2), \qquad (41)
\end{aligned}
$$

$$
g(m_{\tilde{t}_1}^2, m_{\tilde{t}_2}^2) = 2 - \frac{m_{\tilde{t}_1}^2 + m_{\tilde{t}_2}^2}{m_{\tilde{t}_1}^2 - m_{\tilde{t}_2}^2}\log\frac{m_{\tilde{t}_1}^2}{m_{\tilde{t}_2}^2}. \qquad (42)
$$

---

[1] G. Aad *et al.* [ATLAS Collaboration], Phys. Lett. B **716**, 1 (2012) [arXiv:1207.7214 [hep-ex]].

[2] S. Chatrchyan *et al.* [CMS Collaboration], Phys. Lett. B **716**, 30 (2012) [arXiv:1207.7235 [hep-ex]].

[3] G. Aad *et al.* [ATLAS and CMS Collaborations], Phys. Rev. Lett. **114**, 191803 (2015) [arXiv:1503.07589 [hep-ex]].

[4] J. Wess and J. Bagger, "Supersymmetry and supergravity," Princeton, USA: Univ. Pr. (1992) 259 p.

[5] H. P. Nilles, Phys. Rept. **110**, 1 (1984).

[6] P. Nath, R. L. Arnowitt and A. H. Chamseddine, "Applied N=1 Supergravity," Lectures given at Conference (Trieste Particle Phys.1983:1), NUB-2613.

[7] B. Ananthanarayan, J. Lahiri, P. N. Pandita and M. Patra, Phys. Rev. D **87**, no. 11, 115021 (2013) [arXiv:1306.1291 [hep-ph]].

[8] P. N. Pandita and M. Patra, Phys. Rev. D **89**, 115010 (2014) [arXiv:1405.7163 [hep-ph]].

[9] B. Ananthanarayan, J. Lahiri and P. N. Pandita, Phys. Rev. D **91**, 115025 (2015) [arXiv:1507.01747 [hep-ph]].

[10] A. Djouadi, H. E. Haber and P. M. Zerwas, Phys. Lett. B **375**, 203 (1996) [hep-ph/9602234].

[11] P. Osland and P. N. Pandita, Phys. Rev. D **59**, 055013 (1999) [hep-ph/9806351].

[12] P. Osland and P. N. Pandita, hep-ph/9911295.

[13] P. Osland and P. N. Pandita, hep-ph/9902270.

[14] A. Djouadi, W. Kilian, M. Muhlleitner and P. M. Zerwas, Eur. Phys. J. C **10**, 27 (1999) [hep-ph/9903229].

[15] L. Wu, J. M. Yang, C. P. Yuan and M. Zhang, Phys. Lett. B **747**, 378 (2015), [arXiv:1504.06932 [hep-ph]].

[16] J. R. Ellis, G. Ridolfi and F. Zwirner, Phys. Lett. B **262**, 477 (1991).

[17] Y. Okada, M. Yamaguchi and T. Yanagida, Prog. Theor. Phys. **85**, 1 (1991).

[18] H. E. Haber and R. Hempfling, Phys. Rev. Lett. **66**, 1815 (1991).

[19] M. Carena, J. R. Espinosa, M. Quiros and C. E. M. Wagner, Phys. Lett. B **355** (1995) 209.

[20] H. E. Haber, R. Hempfling and A. H. Hoang, Z. Phys. C **75**, 539 (1997).

[21] M. Carena, H. E. Haber, S. Heinemeyer, W. Hollik, C. E. M. Wagner and G. Weiglein, Nucl. Phys. B **580**, 29 (2000).

[22] T. Li, Phys. Lett. B **728**, 77 (2014) [arXiv:1309.6713 [hep-ph]].

[23] P. N. Pandita, Phys. Lett. B **151**, 51 (1985).

[24] E. Boos, A. Djouadi, M. Muhlleitner and A. Vologdin, Phys. Rev. D **66**, 055004 (2002) [hep-ph/0205160].

[25] E. Boos, A. Djouadi and A. Nikitenko, Phys. Lett. B **578**, 384 (2004) [hep-ph/0307079].

[26] N. D. Christensen, T. Han and S. Su, Phys. Rev. D **85**, 115018 (2012) [arXiv:1203.3207 [hep-ph]].

[27] H. E. Haber, hep-ph/9510412.

[28] B. Bhattacherjee, M. Chakraborti, A. Chakraborty, U. Chattopadhyay and D. K. Ghosh, Phys. Rev. D **93**, 075004 (2016). [arXiv:1511.08461 [hep-ph]].

[29] A. Belyaev, N. D. Christensen and A. Pukhov, Comput. Phys. Commun. **184**, 1729 (2013) [arXiv:1207.6082 [hep-ph]].

[30] A. Djouadi, J. L. Kneur and G. Moultaka, Comput. Phys. Commun. **176**, 426 (2007) [hep-ph/0211331].

[31] V. D. Barger, M. S. Berger, A. L. Stange and R. J. N. Phillips, Phys. Rev. D **45**, 4128 (1992).

[32] M. Brucherseifer, R. Gavin and M. Spira, Phys. Rev. D **90**, 117701 (2014) [arXiv:1309.3140 [hep-ph]].

[33] G. Pocsik and G. Zsigmond, Z. Phys. C **10**, 367 (1981).

[34] J. F. Gunion *et al.*, Phys. Rev. D **38**, 3444 (1988).

[35] S. Schael *et al.* [ALEPH and DELPHI and L3 and OPAL and SLD and LEP Electroweak Working Group and SLD Electroweak Group and SLD Heavy Flavour Group Collaborations], Phys. Rept. **427**, 257 (2006), [hep-ex/0509008].